Insights into the Photosensitive Activity of Monolayer HNb$_3$O$_8$ Nanosheets Under Visible Light Irradiation

[1,2]Jinhua Xiong*, [1]Jiahang Chen, [1]Xueqing Shao, [1]Xiuzhen Liu, [1]Lingyan Fu

[1]Fujian Provincial Key Laboratory of Clean Energy Materials, Longyan University,
Longyan 364000, P. R. China.
[2]State Key Laboratory of Photocatalysis on Energy and Environment, Fuzhou University,
Fuzhou 350002, P. R. China.
xjh970996937@sina.com*

Summary: Monolayer HNb$_3$O$_8$ nanosheets, as a platform, were prepared for investigating the mechanism of photosensitized degradation of RhB. We found that RhB molecules were capable to absorb on HNb$_3$O$_8$ nanosheets via a strong interaction between the –N(Et)$_2$ group in RhB molecules and surface Lewis acid sites on HNb$_3$O$_8$ nanosheets, contribution to an easier oxidation of RhB molecules. Thanks to the suitable conduction band of HNb$_3$O$_8$ nanosheets, electrons transferred from excited RhB to HNb$_3$O$_8$ nanosheets effectively and reduced the dissolved O$_2$ in the reaction solution into O$_2$$^{\cdot-}$ immediately, resulting in the efficient photosensitized degradation of RhB.

Key words: HNb$_3$O$_8$ nanosheets; Photosensitization; Mechanism; Electron transfer.

Introduction

Along with the development of the society, dyes are becoming a main organic pollution source, which badly threatens the sustainable development of the ecosystem. Over the past decades, semiconductor photocatalysis has shown a promising prospect in the remediation of environment [1]. It's widely known that there are two approaches to realize the decomposition of dyes over semiconductor photocatalysts. One is that the semiconductors under band-gap excited will produce powerfully active species to oxidize the dyes directly, such as hydroxyl radical and superoxide radical [2]. The other is photosensitive degradation initiated via surface electron injection from the adsorbed dye molecules [3]. Recently, photosensitization has drawn enormous attentions in treatment of dyes pollutions, because of its facility and high efficiency of light energy utilization [4]. As a matter of fact, photosensitization must satisfy a prerequisite condition that electrons can transfer from excited dye molecule to the semiconductor efficiently and the injected electrons can be trapped by O$_2$ to generate O$_2$$^{\cdot-}$, which depends on the redox potential of dyes in the excited state, conduction band of the semiconductor as well as the surface interaction between dyes and the semiconductor. Although, quite a lot of researches about photosensitized degradation of dyes have been carried out, traditional bulk catalysts make it disadvantaged to

Fig out the sensitization process because of the complex catalytic model. As Xie's researches showed [5-7], to gain in-depth atomic-level understanding on mechanism and increase catalytic active sites of heterogeneous catalytic reaction, it would be rather vital to simplify the catalyst model. Crystallographic theory demonstrates that catalyst with monolayer thickness endow a simplest surface atomic structure and a highest surface-to-volume ratio [8]. Hence, development of a novel monolayer semiconductor is a promising strategy to investigate the sensitization process at the molecular level. As we reported before [9, 10], monolayer HNb$_3$O$_8$ nanosheets had a stable crystal structure, suitable conduction band edge (-1.02 V vs SHE, pH=7) and wide band gap (3.68 eV), which made it a desired candidate for the study of sensitization [9, 10]. Herein, we prepared monolayer HNb$_3$O$_8$ nanosheets as the platform for investigating the mechanism of photosensitive degradation, Rhodamine B (RhB) as the probe molecule. It was found that RhB was able to be degraded over HNb$_3$O$_8$ nanosheets via photosensitization, resulting from the strong interaction between RhB molecules and HNb$_3$O$_8$ nanosheets, effective electron injection from excited RhB molecules to HNb$_3$O$_8$ nanosheets and the formation of superoxide radical with powerful oxidation capacity.

---

*To whom all correspondence should be addressed.

Experiment

Preparation of photocatalyst

Monolayer HNb_3O_8 nanosheets (HNb_3O_8-NS) were prepared by a top-down process followed as we have reported before [9].

Characterization

Fourier transform infrared (FTIR) spectra of the samples were performed on a Nicolet Nexus 670 FTIR spectrometer at a resolution of 4 cm^{-1}. Zeta potential test was performed by a Zetasizer 3000 instrument (Malvern Co., UK). DMPO–O_2^- spin-trapping electron paramagnetic resonance (EPR) signals were recorded with a Bruker A300 spectrometer at room temperature. Firstly, 5 mg of HNb_3O_8 nanosheet powders were dispersed well in 0.5 mL of 20 ppm of RhB aqueous and then 15 μL DMPO was added into the mixture solution. Secondly, the samples were encapsulated into capillary tube via siphon syphonage. Finally, the capillary tube was transfer to EPR tube and irradiated under visible light (λ>420 nm). The electrochemical measurements were conducted on an electrochemical workstation (CHI660E) with a conventional three-electrode system, a working electrode, a platinum wire counter electrode and saturated calomel electrode (SCE) as a reference electrode. The working electrode was prepared on fluorine doped tin oxide (FTO) glass followed our previous work [10]. Typically, 5 mg of HNb_3O_8 nanosheets were dispersed in 0.5 ml deionized water by sonicating for at least 10 h to form a homogeneous ink. 15 μL of the dispersion was loaded onto a working electrode with an area of 0.25 cm^2. Linear sweep voltammetry (LSV) was carried out with a scan rate of 25 mV s^{-1}. 0.2 M Na_2SO_4 aqueous solution with/without RhB (the concentration of RhB was set to 20 ppm, when necessary) was used as electrolyte. For example, the LSV test for "HNb_3O_8-NS+20 ppm RhB+light (λ>420 nm)", it means the working electrode loaded with HNb_3O_8-NS was immersed in 0.2 M Na_2SO_4 aqueous solution with 20 ppm RhB. During the LSV test, the working electrode was irradiated with light (λ>420 nm). The working electrode was kept steady for 40 s before the measurement. A 300 W Xenon lamp with a filter at 420 nm was used as a light source.

Photocatalytic Test

The photocatalytic reactions were carried

out as following. Typically, 50 mg photocatalyst were added into 80 mL of 20 ppm RhB aqueous solution in a 100 mL glass container. The mixture solution was dispersed well by ultrasonication and stirred under dark for 2 h to ensure the establishment of adsorption/desorption equilibrium. The suspension was then irradiated under the visible light (λ≥420 nm) by using a 300 W Xenon lamp (PLS-SXE300C, Perfectlight Co., Beijing) with a 420 nm cut-off filter. During the photocatalytic reaction, 1.5 mL of the solution was extracted, every 10 mins, for detecting the variation of the concentration of RhB, via Uv-visible absorption spectra (Cary-50 UV-visible spectrometer).

Results and Discussions

Fig. 1 demonstrated the UV-vis absorption spectral changes of the RhB aqueous solution over monolayer HNb_3O_8 nanosheets under visible light irradiation (λ≥420 nm). As with the increasing time of irradiation, the maximum absorption peak of the solution shifted from 556 to 498 nm and gradually declined to about zero. Based on literature reports, it indicated that RhB suffered from the N-deethylation and the cleavage of the conjugated chromophore structure simultaneously [11]. Blank experiments including "dark with HNb_3O_8 nanosheets" and "light without HNb_3O_8 nanosheets" were performed and no significant variations were found. It verified RhB was indeed decomposed by photocatalysis. However, as we reported before, the HNb_3O_8 nanosheets was only excited under ultraviolet light irradiation because of the wide band gap (E_g) of 3.68 eV [9]. Hence, we deduced the photocatalytic activity for degradation of RhB over HNb_3O_8 nanosheets under visible-light irradiation arose from the photosensitization.
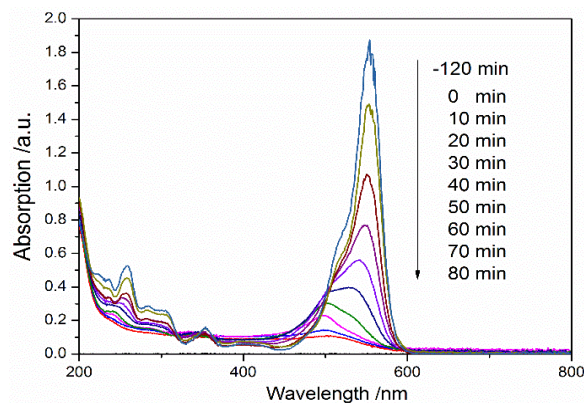

Fig. 1: The temporal evolution curve of Uv-vis absorption spectra of RhB aqueous solution over HNb_3O_8-NS.

As well known, degradation of RhB by photosensitization can be achieved, when injected electrons from excited RhB molecules (RhB[*]) to semiconductor with an appropriate conduction band are powerful enough for reducing O_2 to produce $O_2^{-\bullet}$ [3, 4, 12]. To Fig out the photosensitive degradation process of RhB over HNb_3O_8-NS, series experiments including photocurrent, linear sweep voltammetry, DMPO spin-trapping EPR analysis were carried out. As shown in Fig. 2A, no obvious photocurrent was detected in the existence of HNb_3O_8-NS or RhB individually, because HNb_3O_8-NS was unable to be excited ($\lambda > 420$ nm) to produce carriers and the RhB alone in the excited state was lack of an electron sink to induce the separation of photo-generated carriers, respectively. However, photocurrent increased intensively with the coexistence of RhB and HNb_3O_8-NS. This arose from the photo-generated electrons of RhB[*] were trapped by HNb_3O_8-NS, achieving photo-generated electrons injected from RhB[*] to the semiconductor efficiently. It was reported the redox potentials of RhB and RhB* were 0.95 and -1.42 V vs NHE, respectively [13, 14]. Furthermore, we reported before that the conduction band (CB) edge of HNb_3O_8-NS was -1.02 V. Since the energy level of RhB* was higher than the CB edge of HNb_3O_8-NS, the efficient electron injection from RhB* to HNb_3O_8-NS was feasible in thermodynamics. Moreover, EPR technology was used to further verify that the electrons trapped by HNb_3O_8-NS was able to reduce O_2 to generate $O_2^{-\bullet}$. As shown in Fig. 2B, as similarity with the results of photocurrent response experiments, $O_2^{-\bullet}$ generated when RhB and HNb_3O_8-NS coexisted in the system [15, 16]. Hence, it was reasonable to believe that the degradation of RhB over HNb_3O_8-NS suffered from a photosensitive process.
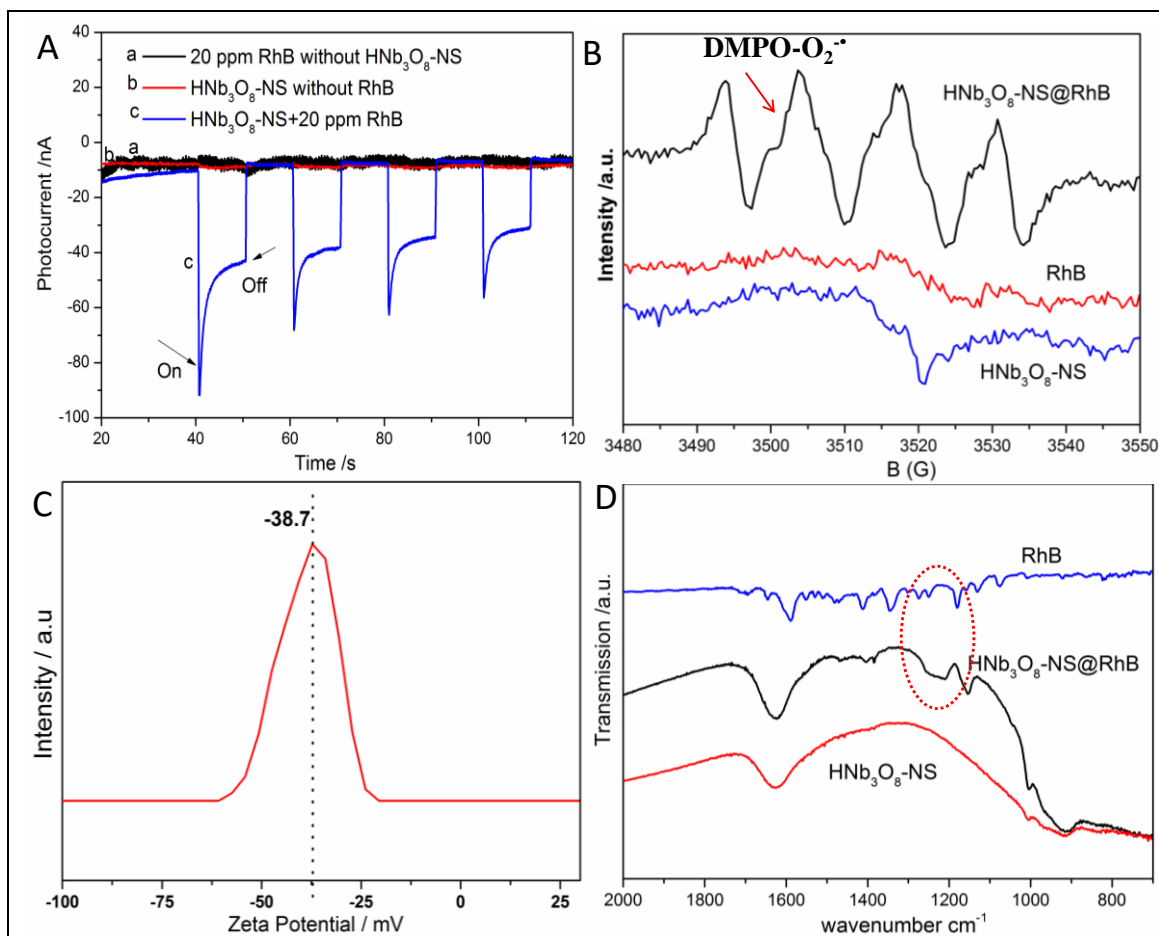

Fig. 2:   A) Transient photocurrent response, B) DMPO spin-trapping EPR spectra of the samples under the irradiation of visible light ($\lambda > 420$ nm), C) Zeta potential of the HNb_3O_8-NS, D) FT-IR spectra of the samples.

To further shed light on the photosensitive process, the interaction between RhB and HNb_3O_8-NS were investigated. As shown in Fig. 2C, HNb_3O_8-NS had a negative zeta potential, which benefitted the adsorption of the cationic RhB via electrostatic interaction. The adsorption behaviour of RhB on the HNb_3O_8-NS was characterized by FT-IR. Fig. 2D showed the FT-IR spectra of RhB, HNb_3O_8-NS and HNb_3O_8-NS@RhB (defined the sample as RhB adsorbed on HNb_3O_8-NS). Compared with the spectra of HNb_3O_8-NS and RhB, HNb_3O_8-NS@RhB sample displayed some new distinctive absorption peak in the region of $1050\sim1250\ cm^{-1}$. This region was assigned to the stretching vibration for C-N bands (v_{C-N}) of $-N(Et)_2$ group in RhB molecules. Broadening and shifting of the absorption peaks arose from the interaction between the Lewis acid sites on HNb_3O_8-NS [17, 18] and lone pair electrons of N in $-N(Et)_2$ group, which affected the bond energy of C-N bands of $-N(Et)_2$ group in RhB molecules. This FT-IR results verified the $-N(Et)_2$ group served as the bridge for the absorption of RhB on HNb_3O_8-NS. To elucidate the positive effect of absorption behaviour on the degradation of RhB over HNb_3O_8-NS, LSV experiments were performed. As shown in Fig. 3A, all the curves exhibited a sharp increased electric current, when electrode potential exceeded 1.3 V vs SCE. This increased electric current resulted from the oxidation of water [19]. After addition of RhB (curve a and b), a new oxidation current appeared on the onset potential about 0.8 V either on the FTO or HNb_3O_8-NS electrode, which arose from the oxidation of RhB on the electrode. Compared with the bare FTO electrode, although HNb_3O_8-NS electrode had a very close onset oxidation potential of RhB, the maximum oxidation limited current was about twice that on the FTO electrode. The increased oxidation limited current was always ascribed to that the efficient adsorption between RhB and HNb_3O_8-NS on the electrode surface promoted the oxidation of RhB. Moreover, when the HNb_3O_8-NS electrode was irradiated with visible light (λ>420 nm, curve c), compared curve c with curve b, the onset oxidation potential for RhB shifted to around 0.7 V, the maximum oxidation limited current increased by about twice and the oxidation half-wave potential lowered approximately 50 mv. It resulted from the RhB adsorbed on HNb_3O_8-NS was excited, and the photo-generated electrons of RhB* were acceleratively extracted under the bias voltage, leading to the easier oxidation of RhB. Therefore, the photocatalytic mechanism over HNb_3O_8 nanosheet was proposed, as shown in Fig. 3B. RhB absorbed on HNb_3O_8 nanosheet was excited under the irradiation of visible light. Electrons transferred from RhB* to HNb_3O_8 nanosheet, accompany with the generation of $O_2^{-\bullet}$. Finally, the RhB$^{+\bullet}$ moleculars were destroyed by $O_2^{-\bullet}$, achieving the degradation of RhB.
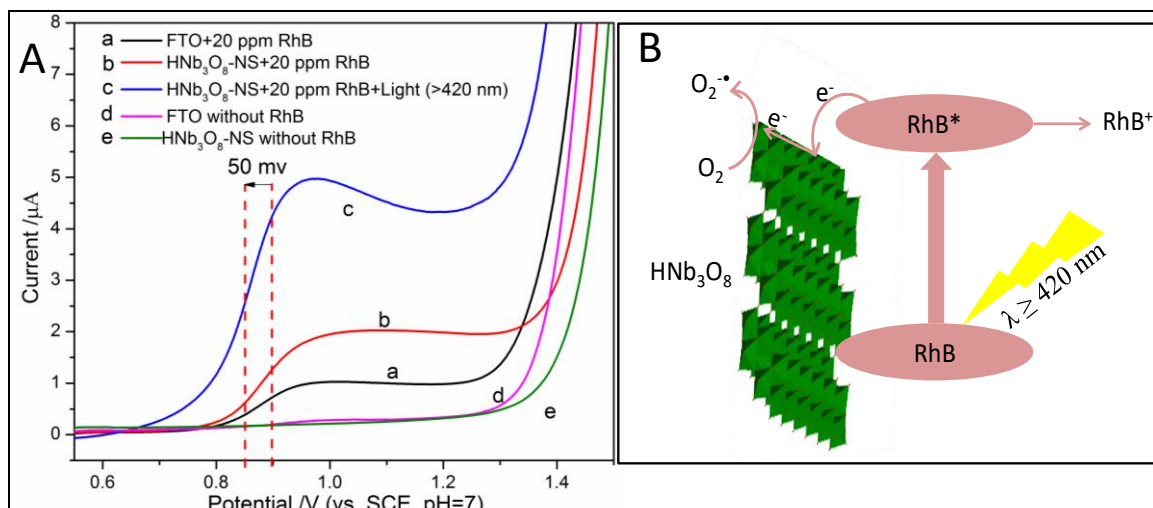

Fig. 3:   A) LSV curves of the work electrodes in different conditions, B) A schematic illustration for degradation of RhB over HNb_3O_8 nanosheet.
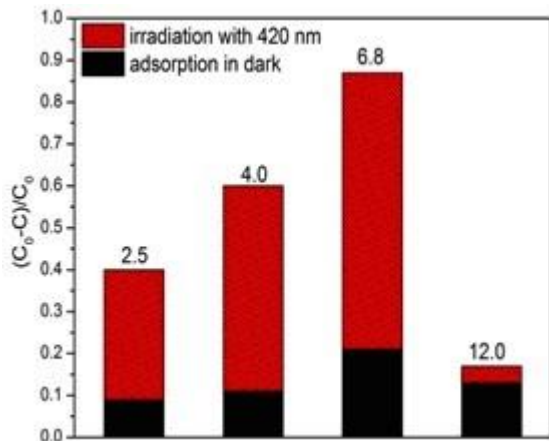
Fig. 4: A) Degradation ratio of RhB over HNb_3O_8-NS with different pH value in 40 mins, B) Degradation of different dyes over HNb_3O_8-NS in 40 mins, (MB=methylene blue, MG=malachite green, MO=methyl orange), C) Degradation ratio of RhB over HNb_3O_8-NS loaded with 1% noble metals (Au, Pd and Pt) in 40 mins, D) Recycle tests for degradation of RhB over HNb_3O_8-NS in 40 mins.

For further elucidate the factors affected the photosensitive degradation of RhB over HNb_3O_8-NS, some controlled experiments were carried out, including varying pH, dyes and photocatalysts, as well as recycle experiments. As shown in Fig. 4A, RhB had a best adsorption ratio (21 %) and degradation ratio (65 %) in pH=6.8. Either the pH increase or decrease, the adsorption and degradation of RhB over HNb_3O_8-NS declined. When RhB was replaced with other cationic dyes such methylene blue (MB) and malachite green (MG) and anionic methyl orange (MO), we found cationic dyes were more inclined to be adsorbed and photosensitive degradation over HNb_3O_8-NS, which probably arose from the fact that surface of HNb_3O_8-NS with negative zeta potential tended to attract the cationic dyes and repulse the anionic dyes via electrostatic interaction. Fig. 4B showed the adsorption ratio and degradation ratio were 68% and 22% for MB, 21% and 41% for MG, 2% and 3% for MO, respectively. Additionally, photocatalyst loaded with noble metal generally availed the enhancement of photocatalytic activity on account to form Mott-schottky junction, which contributed to the transfer and separation of photo-generated

carrier [20]. However, compared with the bare HNb_3O_8-NS, the adsorption and degradation ratios of RhB over HNb_3O_8-NS loaded with 1% of Au, Pd and Pt respectively were all reduced (Fig. 4C). This might be ascribed to the shield effect that the loaded noble covered the photo-sensitive activity sites on HNb_3O_8-NS [21]. These results indicated the adsorption of RhB on HNb_3O_8-NS contributed a lot to the photosensitization. However, unfortunately, we found that photosensitization of RhB over HNb_3O_8-NS declined during the recycle tests (Fig. 4D). To Fig out the reasons, we detected the TOC value of the photosensitive reaction solution. 80 % of the C was still in the solution, even after RhB solution was degraded to colourless. The remained small organic compound competitively adsorbed on HNb_3O_8-NS, leading to the fatal decay of the photosensitive degradation activity of RhB in the next run.

Conclusion

Degradation of RhB over HNb_3O_8-NS was via photosensitization, thanks to the efficient surface electron injection from the RhB* to HNb_3O_8-NS and the formation of $O_2^{-\cdot}$. About 85% of RhB was degraded in 80 mins under visible light irradiation ($\lambda>420$ nm). The adsorption of RhB on HNb_3O_8-NS played a vital role in photosensitization, which benefited the transfer of photo-generated electron from RhB* to HNb_3O_8-NS, leading an easier oxidation of RhB. Nevertheless, it still need some effects to improve the recycle activity for photosensitive degration of RhB over HNb_3O_8-NS in the future work.

Acknowledgements

References

1.   (a) C. Y. Hsiao, C. L. Lee and D. F. Ollis,

Heterogeneous photocatalysis: Degradation of dilute solutions of dichloromethane (CH_2Cl_2), chloroform ($CHCl_3$), and carbon tetrachloride (CCl_4) with illuminated TiO_2 photocatalyst, *J. Catal.,* **82,** 418 (1983); (b) J. Chen, H. Wang, G. Huang, Z. Zhang, L. Han, W. Song, M. Li and Y. Zhang, Facile synthesis of urchin-like hierarchical Nb_2O_5 nanospheres with enhanced visible light photocatalytic activity, *J. Alloy. Compd.,* **728,** 19 (2017).

2. C. S. Turchi and D. F. Ollis, Photocatalytic degradation of organic water contaminants: Mechanisms involving hydroxyl radical attack, *J. Catal.,* **122,** 178 (1990).

3. C. Chen, W. Ma and J. Zhao, Semiconductor-mediated photodegradation of pollutants under visible-light irradiation, *Chem. Soc. Rev.,* **39,** 4206 (2010).

4. J. Hu, W. Fan, W. Ye, C. Huang and X. Qiu, Insights into the photosensitivity activity of BiOCl under visible light irradiation, *Appl. Catal. B: Environ.,* **158-159,** 182 (2014).

5. S. Gao, Z. Sun, W. Liu, X. Jiao, X. Zu, Q. Hu, Y. Sun, T. Yao, W. Zhang, S. Wei and Y. Xie, Atomic layer confined vacancies for atomic-level insights into carbon dioxide electroreduction, *Nat. Commun.,* **8,** 14503 (2017).

6. Y. Sun, S. Gao, F. Lei, C. Xiao and Y. Xie, Ultrathin Two-Dimensional Inorganic Materials: New Opportunities for Solid State Nanochemistry, *Acc. Chem. Res.,* **48,** 3 (2015).

7. Y. Sun, S. Gao, F. Lei and Y. Xie, Atomically-thin two-dimensional sheets for understanding active sites in catalysis, *Chem. Soc. Rev.,* **44,** 623 (2015).

8. S. Bai and Y. Xiong, Recent Advances in Two-Dimensional Nanostructures for Catalysis Applications, *Sci. Adv. Mater.,* **7,** 2168 (2015).

9. J. Xiong, L. Wen, F. Jiang, Y. Liu, S. Liang and L. Wu, Ultrathin HNb_3O_8 nanosheet: an efficient photocatalyst for the hydrogen production, *J. Mater. Chem. A,* **3,** 20627 (2015).

10. J. Xiong, Y. Liu, S. Liang, S. Zhang, Y. Li and L. Wu, Insights into the role of Cu in promoting photocatalytic hydrogen production over ultrathin HNb_3O_8 nanosheets, *J. Catal.,* **342,** 98 (2016).

11. X. Hu, T. Mohamood, W. Ma, C. Chen and J. Zhao, Oxidative Decomposition of Rhodamine B Dye in the Presence of VO^{2+} and/or Pt(IV) under Visible Light Irradiation: N-Deethylation, Chromophore Cleavage, and Mineralization, *J. Phys. Chem. B,* **110,** 26012 (2006).

12. H. Fu, C. Pan, W. Yao and Y. Zhu, Visible-Light-Induced Degradation of Rhodamine B by Nanosized Bi_2WO_6, *J. Phys. Chem. B,* **109,** 22432 (2005).

13. Z. Xiong, L. Zhang, J. Ma and X. Zhao, Photocatalytic degradation of dyes over graphene–gold nanocomposites under visible light irradiation, *Chem. Commun.,* **46,** 6099 (2010).

14. T. Shen, Z. Zhao, Q. Yu and H. Xu, Photosensitized reduction of benzil by heteroatom-containing anthracene dyes, *J. Photoch. Photobio. A,* **47,** 203 (1989).

15. S. Liang, R. Liang, L. Wen, R. Yuan, L. Wu and X. Fu, Molecular recognitive photocatalytic degradation of various cationic pollutants by the selective adsorption on visible light-driven $SnNb_2O_6$ nanosheet photocatalyst, *Appl. Catal. B: Environ.,* **125,** 103 (2012).

16. (a) J. Xiong, Y. Liu, C. Cao, L. Shen, W. Wu, S. Liang, R. Liang and L. Wu, An architecture of $CdS/H_2Ti_5O_{11}$ ultrathin nanobelt for photocatalytic hydrogenation of 4-nitroaniline with highly efficient performance, *J. Mater. Chem. A,* **3,** 6935 (2015); (b) J. Chen, H. Wang, Z. Zhang, L. Han, Y. Zhang, F. Gong, K. Xie, L. Xu, W. Song and S. Wu, Ultrathin HNb_3O_8 nanosheets with oxygen vacancies for enhanced photocatalytic oxidation of amines under visible light irradiation, *J. Mater. Chem. A,* **7,** 5493 (2019).

17. A. Takagaki, M. Sugisawa, D. Lu, J. Kondo, M. Hara, K. Domen and S. Hayashi, Exfoliated nanosheets as a new strong solid acid catalyst, *J. Am. Chem. Soc.,* **125,** 5479 (2003).

18. S. Liang, L. Wen, S. Lin, J. Bi, P. Feng, X. Fu and L. Wu, Monolayer HNb_3O_8 for Selective Photocatalytic Oxidation of Benzylic Alcohols with Visible Light Response, *Angew. Chem. Int. Ed.,* **53,** 2951 (2014).

19. Y. Liu, H. Cheng, M. Lyu, S. Fan, Q. Liu, W. Zhang, Y. Zhi, C. Wang, C. Xiao, S. Wei, B. Ye and Y. Xie, Low Overpotential in Vacancy-Rich Ultrathin $CoSe_2$ Nanosheets for Water Oxidation, *J. Am. Chem. Soc.,* **136,** 15670 (2014).

20. J. Yang, D. Wang, H. Han and C. Li, Roles of Cocatalysts in Photocatalysis and Photoelectrocatalysis, *Acc. Chem. Res.,* **46,** 1900 (2013).

21. W. Foo, C. Zhang and G. Ho, Non-noble metal Cu-loaded TiO_2 for enhanced photocatalytic H_2 production, *Nanoscale,* **5,** 759 (2013).